Growth and depth dependence of visible luminescence in wurtzite InN epilayers

X. D. Pu, W. Z. Shen,[a] and Z. Q. Zhang
Laboratory of Condensed Matter Spectroscopy and Opto-Electronic Physics, Department of Physics, Shanghai Jiao Tong University, 1954 Hua Shan Road, Shanghai 200030, People's Republic of China

H. Ogawa and Q. X. Guo
Department of Electrical and Electronic Engineering, Faculty of Science and Engineering, Saga University, Saga 840-8502, Japan

(Received 20 November 2005; accepted 24 February 2006; published online 10 April 2006)

We present detailed investigation of growth and depth dependence of visible (~1.9 eV) photoluminescence (PL) in wurtzite InN epilayers grown by magnetron sputtering. For normal surface incidence, PL peak was found to redshift with increasing growth temperatures. Cross-sectional PL measurements were able to separate contributions from the InN epilayers and sapphire substrates, which not only demonstrated the visible luminescence in InN but also revealed the blueshift of the PL peak with laser spot focusing from epilayer surface toward the interface. The results have been well explained by the growth mechanism and residual strain along growth direction of InN epilayers. © *2006 American Institute of Physics*. [DOI: 10.1063/1.2193059]

As a promising semiconductor among group III-nitride compounds, indium nitride (InN) has recently received intensive research interest. However, the growth of high quality InN remains a formidable challenge due to the low dissociation temperature of InN and the extremely high equilibrium vapor pressure of nitrogen. Many of its fundamental properties are still not well known despite the detailed investigation since the 1980s. Current research interests are on the origin of the infrared (~0.7 eV) photoluminescence (PL) peak and the epilayer depth dependence of the electrical and optical properties in hexagonal InN.

The observed infrared PL and optical absorption in InN (Refs. 1–3) were considered as unambiguous evidence for the revision of fundamental band gap energy from the long-time established ~1.9 eV (Ref. 4) to the narrow gap nature of ~0.7 eV for hexagonal InN. However, our recent observation of strong room temperature visible luminescence at 1.87 eV, together with a clear absorption edge at 1.97 eV, has demonstrated that it is not accurate in the assignment of ~0.7 eV band gap for intrinsic InN simply from the coincidence of the PL and absorption data.[5] Actually, it is still controversial in the literature for the origin of ~0.7 eV PL transition and therefore the fundamental band gap energy in InN. The infrared PL peak has been attributed to In clustering in InN epilayers,[6] exciton emissions in In-rich interfaces,[7] and an extrinsic recombination process analogous to the processes that give the blue band in AlN and the yellow band in GaN.[8] Recently, Ho *et al.*[9] have confirmed that the observed infrared PL peak is not consistent with the band-edge transition in InN. Correspondingly, the possibility of an ~1.2 eV band gap has been rebuilt for InN,[8,10] and the resonant Raman measurements on the InN with ~0.7 eV luminescence have also indicated clearly the presence of an InN critical point within ~0.2–0.3 eV below 1.5 eV.[11] We have extracted the band gap of ~1.2 eV in InN from the PL and optical transmission spectra.[12]

Another interesting topic is surface and interface properties of InN epilayers. Mahboob *et al.*[13] have found a maximum electron density occurs near the surface of InN epilayers, and it gradually declines to the bulk value, confirming the observation of surface charge accumulation by capacitance-voltage measurements.[14] Swartz *et al.*[15] have identified surface/interface and bulk conduction mechanisms in InN through the variable magnetic field Hall measurements. For optical properties, Chen *et al.*[16] have employed the cross-sectional Raman spectra to detect the existence of residual strain along the growth direction of the InN epilayers.

The studied InN thin films were grown on (0001) α-Al_2O_3 substrates by reactive radio frequency magnetron sputtering.[5] Two sets of InN samples were employed in the present investigation. For the first set (A series), the InN epilayers were grown directly on the α-Al_2O_3 substrates with the growth temperature from 100 to 500 °C (A1: 100 °C, A2: 200 °C, A3: 300 °C, A4: 400 °C, and A5: 500 °C), while the second set (B series) InN epilayers were deposited on 10 nm AlN buffer layers under the same substrate temperature (B1: 100 °C, B2: 200 °C, B3: 300 °C, B4: 400 °C, and B5: 500 °C). The thickness of these InN epilayers varies from 1.4 to 2.5 μm. Micro-PL and Raman measurements were performed on a Jobin Yvon LabRAM HR 800 micro-Raman system equipped with an Andor DU420 classic charge-coupled device (CCD) detector. The employment of a 100× optical microscopy objective with a numerical aperture of 0.9 will yield a laser spot size of ~0.6 μm under an Ar^+ laser (514.5 nm). The optical transmission measurements were carried out on a Jobin Yvon 460 monochromator.

Figure 1(a) shows a typical x-ray diffraction (XRD) (by Bruker D8 ADVANCE system with a Cu $K\alpha_1$ line) profile of the InN thin film B1. Only the peak from (0002) InN is observed except the peak of the (0006) reflection from the α-Al_2O_3 substrate. It indicates that the c axis of InN with a wurtzite structure is perpendicular to the substrate surface of (0001) α-Al_2O_3. Figure 1(b) displays the corresponding room temperature Raman spectrum with the laser normal incidence to surface. We can identify the clear phonon modes

[a]Author to whom correspondence should be addressed; electronic mail: wzshen@sjtu.edu.cn

 © 2006 American Institute of Physics
Downloaded 10 Apr 2006 to 202.120.52.61. Redistribution subject to AIP license or copyright, see http://apl.aip.org/apl/copyright.jsp

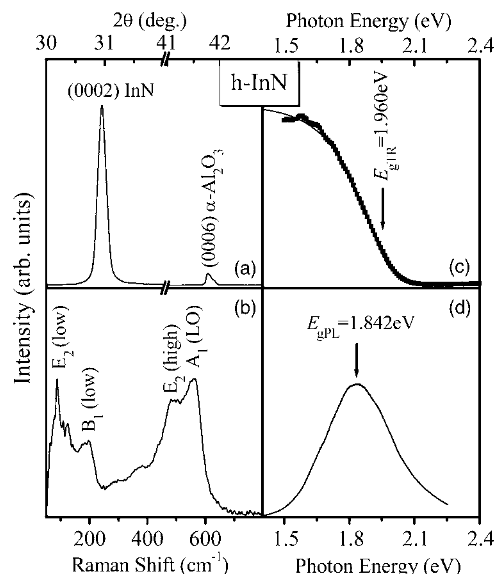

FIG. 1. (a) XRD, (b) Raman, (c) optical transmission, and (d) PL spectra of the wurtzite InN thin film B1 at room temperature. For Raman and PL measurements, laser light is focused on InN epilayer surface.

for hexagonal InN: E_2(low), B_1(low), E_2(high), and A_1 [longitudinal optical (LO)].[17] Figures 1(c) and 1(d) show the optical transmission and PL spectra (with the laser normal incidence to surface) of the InN sample B1 at room temperature. By the aid of a detailed calculation of the transmission profile considering both the intrinsic square-root absorption and Urbach exponential absorption edge,[18] we are able to demonstrate a fairly good agreement between the calculated solid curve and experimental data (solid squares), yielding the transmission energy $E_{g\mathrm{TR}}$ of 1.960 eV and Urbach bandtail parameter E_U of 117 meV. Moreover, it is interesting to note that the present InN exhibits a strong room temperature visible luminescence with the emission peak at 1.842 eV (without any luminescence signal around 0.7 eV).

It should be noted that transition metals present in sapphire substrates can contribute PL in the region of interest.[19] However, our cross-section PL measurements have ruled out that possibility by separating contributions from the InN epilayers and sapphire substrates. Figure 2 presents the depth dependence of the room temperature PL spectra from the InN samples A1 and B1 (both with thickness of 2.5 μm) under laser light incidence on cross section instead of surface. The inset of Fig. 2 displays a cross-sectional image taken with a CCD camera, where $Z=0$ μm represents the surface of InN epilayer, and $Z=2.5$ μm for InN(AlN)/sapphire interface. As the laser spot probes deeper from the surface toward substrate, a clear blueshift of the PL peaks (marked by arrows) can be observed. When the laser spot focuses at $Z=2.4$ μm (i.e., the InN(AlN)/sapphire interface), we can identify the luminescence contribution of both InN epilayer and α-Al_2O_3 substrate simply from the PL line shape and peak, where we have deconvoluted these two emission bands by two dotted curves. At further deeper focus, the luminescence becomes totally from the α-Al_2O_3 substrate.

Due to high electron concentration ($\sim 10^{20}$ cm^{-3}), InN thin films are in a degenerate condition. The Stokes shift of $\sim$0.1 eV between $E_{g\mathrm{TR}}$ and PL peak in Fig. 1 can be explained by different requirements for the momentum selection rule between the absorption and luminescence.[5,12] Nevertheless, the coincidence between the PL peak and

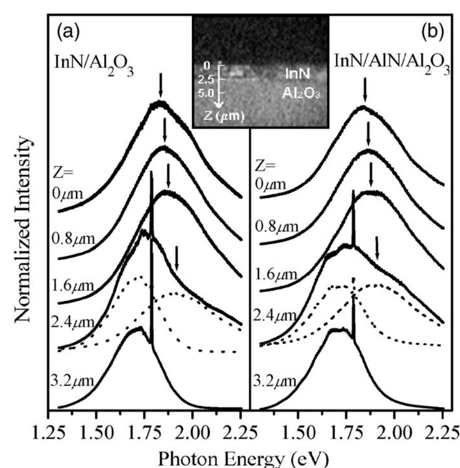

FIG. 2. Depth dependence of normalized room temperature PL spectra from InN samples (a) A1 and (b) B1 under the laser light incidence on the cross section, with CCD camera image shown in the inset.

transmission energy does not indicate the fundamental band gap of $\sim$1.9 eV for intrinsic InN.[5] For free electron concentration of $\sim 10^{20}$ cm^{-3}, the investigated samples should have a correction of $\sim$0.6–0.7 eV for the Burstein-Moss shift, band gap renormalization, and Urbach bandtail effects,[12] resulting in the $\sim$1.2 eV fundamental band gap for intrinsic InN. Butcher *et al.*[20] have recently provided a direct measure of the absolute maximum extent of the Burstein-Moss effect in InN and obtained a value of $\sim$0.72 eV for InN with room temperature carrier concentration of 5×10^{20} cm^{-3} and band-edge absorption of 1.88 eV, also indicating a fundamental band gap of $\sim$1.2 eV.

Figures 3(a) and 3(a′) display the PL (with the laser normal incidence to surface) peak energies of these two sets of InN samples, together with their corresponding full width at half maxima (FWHM) in Figs. 3(b) and 3(b′). Obviously, both PL peak and FWHM decrease with increasing substrate temperatures. We also show the growth temperature dependence of the Urbach band tail parameter E_U [in Figs. 3(c) and 3(c′), obtained by calculating the optical transmission spectra as shown in Fig. 1(c)]. The Urbach band tail parameter E_U mainly reveals the structural disorder in InN samples.[18] The decrease in PL FWHM and E_U clearly indicates the crystallinity quality of the InN samples improves with the growth temperature. The experimental data in Fig. 3 also

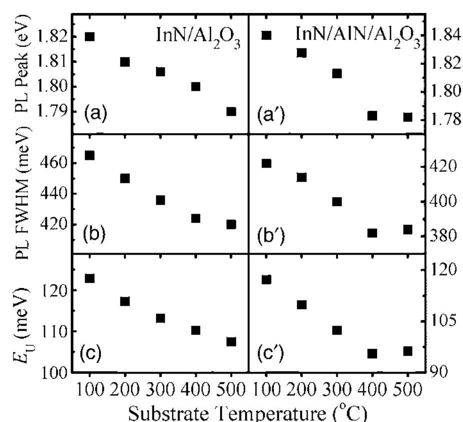

FIG. 3. Growth temperature dependence of the room temperature luminescence [(a) and (a′)] peak energy and [(b) and (b′)] FWHM under laser normal incidence to surface, together with the corresponding [(c) and (c′)] Urbach bandtail parameter E_U from the optical transmission spectra.

Downloaded 10 Apr 2006 to 202.120.52.61. Redistribution subject to AIP license or copyright, see http://apl.aip.org/apl/copyright.jsp

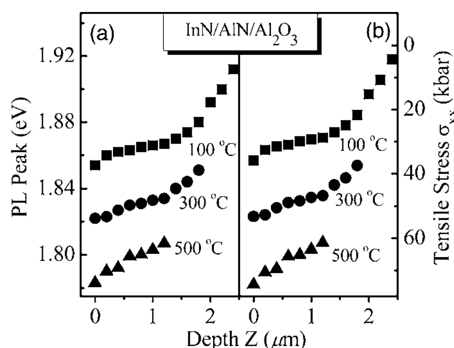

FIG. 4. Cross-sectional depth dependence of (a) luminescence peak energy and (b) estimated stress in InN epilayers (samples B1, B3, and B5) with the surface beginning at $Z=0$ μm.

clearly reveal the improvement of InN epilayer structure with the AlN buffer layers, which is largely due to the isomorphism of the epitaxial AlN buffer layer and InN epilayer.

With increasing substrate temperatures, the decrease in the PL peak energy in Figs. 3(a) and 3(a′) could be attributed, at first sight, to the decrease of high free electron concentration, relevant with the improvement of InN crystallinity. However, our careful Hall effect measurements do not show the correspondence. The depth dependence of the PL peak energy shown in Fig. 2 also does not follow the reported spatial variation of electron concentration within InN epilayers.[13,14] Another important influential factor is the residual strain along the growth direction of InN epilayers, which is both growth temperature and film depth dependent.

In-plane tensile (compressive) stress within the InN epilayer will redshift (blueshift) the luminescence peak in InN. Mainly, there are three kinds of stresses in thin films. The lattice-mismatch strain is normally relieved when the epilayer thickness in our samples is far beyond the critical thickness. During the period of postgrowth cooling, thermal strain appears due to the different thermal expansion coefficients between the epilayer and substrate. Since the thermal expansion coefficient of InN $(3.8\times10^{-6}/\mathrm{K})$ is smaller than that of both AlN $(4.2\times10^{-6}/\mathrm{K})$ and α-Al_2O_3 $(7.5\times10^{-6}/\mathrm{K})$, we therefore expect a compressive stress for the thermal strain in both A and B series samples, and the compressive stress in A series samples will be much larger than that of B series ones. Meanwhile, another stress occurs due to the differential cooling rate along the cross section of the sample (called cooling strain). The fastest cooling rate on the epilayer surface results in the largest tensile stress, which gradually declines toward the interface. Both the thermal and cooling strains in epilayers increase with the growth temperature, and the observed redshift of the PL peak in Fig. 3 reveals the gradual dominant contribution of the tensile cooling strain at surface of the epilayers. In comparison with B series samples, the weaker surface residual tensile stress in A series ones due to the compensation of larger compressive thermal strain will lead to the smaller redshift of PL peak, as clearly observed in Fig. 3, further verifying the above arguments.

Figure 4(a) displays the typical depth dependence of the peak energies from cross-sectional PL spectra of InN epilayers (B series). In addition to the redshift of PL peak with increasing substrate temperatures, we see clear blueshift of the PL peaks along the cross section from the epilayer surface ($Z=0$ μm) to interface. For the compressive thermal strain, it increases with the depth Z, and would be the greatest near the interface. However, the cooling strain has largest tension at epilayer surface, and gradually declines toward the interface. The compensation between the compression and tension yields the decrease in the residual tensile strain within the epilayers toward the interface, and therefore the blueshift of the PL peaks in Figs. 2 and 4(a). In contrast, the reported decrease in electron concentration with the depth in InN can only result in redshift of the PL peaks. Furthermore, we can apply the conventional elastic theory for relationship between the measured peak energy $E_{g\mathrm{PL}}$ and in-plane strain ε_H via $E_{g\mathrm{PL}}=E_{g\mathrm{PL}0}+\alpha\varepsilon_H$, with $E_{g\mathrm{PL}0}$ ($\sim$1.92 eV) the PL peak energy in unstrained InN thin films and deformation potential α [$\sim$−4.1 eV (Ref. 21)]. Figure 4(b) shows the estimated in-plane stress σ_{xx} with the elastic constants in Ref. 22. It is clear that InN epilayers grown on sapphire substrates are under tension with stress values up to 74 kbars depending on the growth temperature and sample thickness.

This work was supported in part by the National Natural Science Foundation of China under Contract Nos. 10125416 and 60576067, PCSIRT, the Grant-in-Aid for Scientific Research (c) (No. 16560013) from the Ministry of Education, Culture, Sports, Science, and Technology, Japan, and the Venture Business Laboratory of Saga University.

[1]V. Yu. Davydov, A. A. Klochikhin, R. P. Seisyan, V. V. Emtsev, S. V. Ivanov, F. Bechstedt, J. Furthmüller, H. Harima, A. V. Mudryi, J. Aderhold, O. Semchinova, and J. Graul, Phys. Status Solidi B **229**, R1 (2002).
[2]J. Wu, W. Walukiewicz, K. M. Yu, J. W. Ager III, E. E. Haller, H. Lu, W. J. Schaff, Y. Saito, and Y. Nanishi, Appl. Phys. Lett. **80**, 3967 (2002).
[3]T. Matsuoka, H. Okamoto, M. Nakao, H. Harima, and E. Kurimoto, Appl. Phys. Lett. **81**, 1246 (2002).
[4]T. L. Tansley and C. P. Foley, J. Appl. Phys. **59**, 3241 (1986).
[5]Q. X. Guo, T. Tanaka, M. Nishio, H. Ogawa, X. D. Pu, and W. Z. Shen, Appl. Phys. Lett. **86**, 231913 (2005).
[6]T. V. Shubina, S. V. Ivanov, V. N. Jmerik, D. D. Solnyshkov, V. A. Vekshin, P. S. Kop″ev, A. Vasson, J. Leymarie, A. Kavokin, H. Amano, K. Shimono, A. Kasic, and B. Monemar, Phys. Rev. Lett. **92**, 117407 (2004).
[7]D. Alexandrov, K. Scott, K. S. A. Butcher, and M. Wintrebert-Fouquet, J. Vac. Sci. Technol. A **22**, 954 (2004).
[8]O. Briot, B. Maleyre, S. Clur-Ruffenach, B. Gil, C. Pinquier, F. Demangeot, and J. Frandon, Phys. Status Solidi C **1**, 1425 (2004).
[9]J. C. Ho, P. Specht, Q. Yang, X. Xu, D. Hao, and E. R. Weber, J. Appl. Phys. **98**, 093712 (2005).
[10]K. S. A. Butcher, *Preface for the Proceedings of the First International Indium Nitride Workshop, Fremantle, Australia*, 16–20 November 2003 [J. Cryst. Growth **269**, vii (2004)].
[11]M. Kuball, J. W. Pomeroy, M. Wintrebert-Fouquet, K. S. A. Butcher, H. Lu, W. J. Schaff, T. V. Shubina, S. V. Ivanov, A. Vasson, and J. Leymarie, Phys. Status Solidi A **202**, 763 (2005).
[12]W. Z. Shen, X. D. Pu, J. Chen, H. Ogawa, and Q. X. Guo, Solid State Commun. **137**, 49 (2006).
[13]I. Mahboob, T. D. Veal, C. F. McConville, H. Lu, and W. J. Schaff, Phys. Rev. Lett. **92**, 036804 (2004).
[14]H. Lu, W. J. Schaff, L. F. Eastman, and C. E. Stutz, Appl. Phys. Lett. **82**, 1736 (2003).
[15]C. H. Swartz, R. P. Tompkins, N. C. Giles, T. H. Myers, H. Lu, W. J. Schaff, and L. F. Eastman, J. Cryst. Growth **269**, 29 (2004).
[16]J. W. Chen, Y. F. Chen, H. Lu, and W. J. Schaff, Appl. Phys. Lett. **87**, 041907 (2005).
[17]Z. G. Qian, W. Z. Shen, H. Ogawa, and Q. X. Guo, J. Phys.: Condens. Matter **16**, R381 (2004).
[18]W. Z. Shen, L. F. Jiang, H. F. Yang, F. Y. Meng, H. Ogawa, and Q. X. Guo, Appl. Phys. Lett. **80**, 2063 (2002).
[19]K. S. A. Butcher and T. L. Tansley, Superlattices Microstruct. **38**, 1 (2005).
[20]K. S. A. Butcher, H. Hirshy, R. M. Perks, M. Wintrebert-Fouquet, and P. P.-T. Chen, Phys. Status Solidi A **203**, 66 (2006).
[21]N. E. Christensen and I. Gorczyca, Phys. Rev. B **50**, 4397 (1994).
[22]A. F. Wright, J. Appl. Phys. **82**, 2833 (1997).

Downloaded 10 Apr 2006 to 202.120.52.61. Redistribution subject to AIP license or copyright, see http://apl.aip.org/apl/copyright.jsp